J Ginseng Res 44 (2020) 738–746

Contents lists available at ScienceDirect

Journal of Ginseng Research

journal homepage: http://www.ginsengres.org

Research Article

# Effects of red ginseng on the elastic properties of human skin

Moon Young Park [1,☆], Se Jik Han [1,2,☆], Donggerami Moon [1], Sangwoo Kwon [1], Jin-Woo Lee [3], Kyung Sook Kim [1,*]

[1] Department of Biomedical Engineering, College of Medicine, Kyung Hee University, Seoul, Republic of Korea
[2] Department of Medical Engineering, Graduate school, Kyung Hee University, Seoul, Republic of Korea
[3] Medical Science Research Institute, Kyung Hee University Medical Center, Seoul, Republic of Korea

ARTICLE INFO

*Article history:*
Received 19 February 2019
Received in Revised form
9 August 2019
Accepted 14 August 2019
Available online 21 August 2019

*Keywords:*
Atomic force microscopy
Cellular stiffness
Collagen
Red ginseng
Skin elasticity

ABSTRACT

*Background:* Red ginseng contains components, including microelements, vitamins, essential oils, and fatty acids, that can be used in skincare to delay the aging process. We investigated the effects of red ginseng treatment on skin elasticity by assessing cellular stiffness and measuring collagen protein synthesis.

*Methods:* Human dermal fibroblasts were treated with red ginseng, and the resulting changes in stiffness were investigated using atomic force microscopy. Cytoskeletal changes and mRNA expression of biomarkers of aging, including that of procollagens I and VII, elastin, and fibrillin-1, were investigated. Collagen in a human skin equivalent treated with red ginseng was visualized via hematoxylin and eosin staining, scanning electron microscopy, and atomic force microscopy.

*Results and conclusion:* The stiffness of fibroblasts was significantly reduced by treatment with red ginseng concentrations of $\geq$ 0.8 mg/mL. The ratio of F-actin to G-actin decreased after treatment, which corresponded to a change in fibroblast stiffness. The storage modulus ($G'$) and loss modulus ($G''$) of the skin equivalent were both lowered by red ginseng treatment. This result indicates that the viscoelasticity of the skin equivalent can be restored by red ginseng treatment.

© 2019 The Korean Society of Ginseng. Publishing services by Elsevier B.V. This is an open access article under the CC BY-NC-ND license (http://creativecommons.org/licenses/by-nc-nd/4.0/).

## 1. Introduction

Skin aging results from a combination of endogenous and exogenous factors [1]. Endogenous factors include genes, hormones, and metabolic processes, while exposure to sunlight, pollution, ionizing radiation, chemicals, and toxins is among the exogenous factors. Skin aging is associated with complex changes in the biological, chemical, and mechanical properties of the skin. With aging, pigment-containing cells, called melanocytes, decrease in number and increase in size [2], and the blood vessels of the dermis become more fragile [3]. In addition, the skin becomes dry and uneven and has reduced strength and elasticity [4,5].

The overall skin condition can be evaluated by measuring its elasticity or viscoelasticity. Elasticity is the resistance of a material to deformation by stress, and viscoelastic materials act as both elastic solids and viscous fluids when stressed. Although several methods for objectively measuring the elastic properties of skin have been developed [6,7], it is difficult to measure the mechanical properties of skin, and the methods described to date have not been standardized for use in research or clinical settings.

The elastic properties of skin are linked to cellular stiffness and extracellular matrix components that can be used as aging biomarkers, including collagen, elastin, and fibrillin-1. Cellular elasticity can be measured via atomic force microscopy (AFM), a type of high-resolution scanning microscopy that uses a sharp probe to analyze the surfaces of materials. This method is widely used in biological studies because it enables nanoscale imaging without special sample preparation or deformation and allows for imaging of submerged materials as well as measurement of the elasticity of cells and tissues. Collagen is a major component of the dermis and plays a key role in maintaining the tensile strength of skin [8]. Elastin provides elasticity, but only small quantities of elastin are present in the dermis [9]. Fibrillin-1 is a microfibrillar protein important for the assembly of elastic fibers from elastin [10].

Red ginseng is known to have antiaging effects. Ginseng can protect the epidermal and dermal layers of the skin from strong

* Corresponding author. Department of Biomedical Engineering, College of Medicine, Kyung Hee University, 1 Hoegi-dong, Dongdaemun-gu, Seoul, Republic of Korea.
*E-mail address:* moosou94@khu.ac.kr (K.S. Kim).
☆ Theses authors are contributed equally.

https://doi.org/10.1016/j.jgr.2019.08.004
p1226-8453 e2093-4947/$ – see front matter © 2019 The Korean Society of Ginseng. Publishing services by Elsevier B.V. This is an open access article under the CC BY-NC-ND license (http://creativecommons.org/licenses/by-nc-nd/4.0/).

UV-B radiation [11], while maltol, one of the phenolic compounds present in red ginseng, reduces fatigue and exhibits antioxidant properties [12]. In addition, ginseng extracts, including ginsenosides Re, Rc, and Rb1, induce procollagen type I–related gene expression and decrease that of matrix metalloproteinase 1 and tumor necrosis factor [13]. The potential benefits of treating the skin with red ginseng have been investigated in *in vivo* studies. Lee et al. [14] reported the antiphotoaging effects of red ginseng on hairless SKH-1 mice. In a group of mice treated with red ginseng, epidermal thickness increased and wrinkle formation was inhibited; moreover, there was a decrease in the immunohistochemical density of myeloperoxidase, which is related to inflammation in photoaged skin. Capella and Dietler [15] investigated the effects of ginseng intake on facial skin in women and showed that several parameters improved dose dependently by ginseng intake, including the sebum and moisture content and melanin and erythema indexes.

In this study, we investigated the effects of red ginseng on cellular stiffness and biomarkers of aging by treating human dermal fibroblasts (HDFs) with various red ginseng concentrations and treatment durations. Then, changes in elasticity were analyzed, fibroblast stiffness was measured using AFM, and the mRNA expression levels of procollagen, elastin, and fibrillin-1 were determined. The effects of red ginseng on collagen protein synthesis were investigated in cells and a human skin equivalent, and changes in the red ginseng–induced viscoelasticity of the skin equivalent were also determined.

## 2. Materials and methods

### 2.1. Preparation of red ginseng

Korean Red Ginseng (KRG) was derived from 6-year-old *Panax ginseng* Meyer roots. KRG was extracted in distilled water at 86 °C for 12 h. The extracts were collected and evaporated in a rotary evaporator (Büchi, St. Gallen, Switzerland) at 45 °C to remove the solvent. The KRG water extract was diluted 5-fold with distilled water and freeze-dried to obtain a dry powder.

### 2.2. Analyses of KRG components by ultraperformance liquid chromatography

The ginsenoside content of KRG was analyzed via ultraperformance liquid chromatography (UPLC). Deionized water (25 mL) was added to 1 g of ginseng powder in a beaker, and the diluted ginseng was left at room temperature for 1 h. Next, methanol was added to a total volume of 50 mL, and this was extracted for 30 min at 60 Hz in an ultrasonic cleaner (Wiseclean, Seoul, South Korea). The solution was filtered (0.2-μm filter; Acrodisk, Port Washington, NY, USA) and injected into the UPLC system. UPLC analyses were performed using water (Waters Corporation, Milford, MA, USA), a sample manager module, and a column heater. Data were collected and processed using Empower chromatography software (Waters Corporation). A UPLC BEH C18 column (2.1 mm × 50 mm; 1.7-μm particles) (Waters Corporation, Seoul, Korea) was used for separation. The column temperature was 40 °C, the flow rate was 0.6 mL/min, and the injection volume was 2 μL. The mobile phase consisted of deionized water (A) and acetonitrile (B). The UPLC gradient conditions were as follows: 0.5–14.5 min (15–30% B), 14.5–15.5 min (15–30% B), 15.5–16.5 min (32–40% B), 16.5–17.5 min (40–30% B), 17.0–21.0 min (55–30% B), 21–25 min (90–15% B), and 25–27 min (15% B). The detection wavelength was set at 203 nm. The total ginsenoside content of KRG was measured using UPLC and a standard ginsenoside sample.

### 2.3. Cell culture and viability

HDFs were purchased from the Korean Cell Line Bank (Seoul, South Korea). The fibroblasts were grown in Dulbecco's modified Eagle's medium supplemented with 10% fetal bovine serum, 2 mM glutamine, and 1% penicillin–streptomycin–amphotericin B (10,000 U/mL, 10 g/mL, and 25 mg/mL, respectively; Gibco, Waltham, MA, USA) at 37 °C in a humidified incubator containing 5% $CO_2$. Cell viability was analyzed as a function of ginseng concentration and treatment time using the 3-(4,5-dimethylthiazol-2-yl)-2,5-diphenyl tetrazolium bromide (Sigma-Aldrich, St. Louis, MO, USA) assay. The cells were plated into wells at a density of $2 \times 10^4$ cells/well. KRG was added to the wells at various concentrations (0, 0.2, 0.4, 0.8, 1.0, and 2.0 mg/mL) and incubated for increasing durations (0, 6, 12, and 24 h). After incubation, EZ-Cytox solution (DoGen Bio, Seoul, Kores) was added to each well at 10 μL/well, and the plates were incubated at 37 °C for 1 h. The absorbance was measured at 450 nm using a Multiskan EX ELISA microplate reader (Thermo Fisher Scientific, Rockford, IL, USA).

### 2.4. Human skin equivalent

The Neoderm®-D human skin equivalent was purchased from TEGO Science (Seoul, South Korea). Neoderm®-D is a three-dimensional skin culture model that can be used instead of experimental animals. The HDFs were cultured in a collagen matrix for 1 day, and keratinocytes were used to seed the matrix. The HDFs and keratinocytes were cocultured in the collagen matrix for 4 days. Next, the collagen matrix embedded with the HDFs and keratinocytes was exposed to air. The human skin equivalent was treated with 0.8 mg/mL KRG for increasing durations (0, 6, 12, and 24 h).

### 2.5. G-actin and F-actin protein levels

The G-actin and F-actin protein levels were measured using the G-/F-actin Biochem *in vivo* assay kit (Cytoskeleton, Inc., Denver, CO, USA). After ultracentrifugation of 100 μL of cell lysates at 100,000 × *g* and 37 °C for 1 h using a 90 Ti rotor (Beckman Instruments, Palo Alto, CA, USA), supernatants containing G-actin were transferred to fresh tubes, and the pellets containing F-actin were resuspended in 100 μL of F-actin depolymerization buffer. For sodium dodecyl sulfate–polyacrylamide gel electrophoresis, 8 μL each of the pellet and supernatant samples were loaded onto 12% polyacrylamide gels. After separation, the protein samples were transferred to polyvinylidene difluoride membranes (Amersham Biosciences, Piscataway, NJ, USA), which were then blocked with 5% nonfat dry milk at room temperature for 1 h. The membranes were incubated with an anti–actin primary antibody (1:500 dilution), washed, and incubated for 1 h with a horseradish peroxidase–conjugated secondary antibody (Cell Signaling Technology, Beverly, MA, USA), diluted 1:2500 in Tris-buffered saline with Tween 20. After a second wash with Tris-buffered saline with Tween 20, the target protein bands were visualized using an enhanced chemiluminescence kit (Thermo Fisher Scientific, MA, USA) and imaged using a Davinch-Chemi Chemiluminescence Imaging System (Davinch-K Co., Seoul, South Korea). To quantify the protein levels, the band densities were measured using ImageJ software (NIH Image, MA, USA).

### 2.6. RNA isolation and real-time polymerase chain reaction

The cells were plated at a density of $3 \times 10^5$ cells/well and incubated for 24 h at 5% $CO_2$. The cells were treated with different concentrations of KRG, and total RNA was isolated from the treated cells using the TRIzol reagent (Thermo Fisher Scientific). First-

**Table 1**
Content of ginsenosides in red ginseng.

| Ginsenosides | Rb1 | Rb2 | Rc | Rd | Rg3s | Rg3r | Re | Rf | Rg1 | Rg2s | Rh1 |
|---|---|---|---|---|---|---|---|---|---|---|---|
| Content (mg/g) | 34.93 | 13.17 | 13.67 | 4.03 | 3.53 | 1.93 | 9.47 | 4.33 | 9.27 | 3.77 | 2.57 |

strand cDNA was synthesized using a reverse transcription system containing 1 mM dNTPs, 1 μg of RNA, 1 × reaction buffer, and 5 μM random primers (Promega, Madison, WI, USA). The primer sequences were as follows: procollagen type I forward, 5′-CTCGAGGTGGACACCACCCT-3′; procollagen type I reverse, 5′-CAGCTGGATGGCCACATCGG-3′ (372 bp); procollagen type VII forward, 5′-GCGAGAGGGGCTTCCCTGGA-3′; procollagen type VII reverse, 5′-CAATGCCACCTTCACCTGGT-3′ (369 bp); elastin forward, 5′-GTTGGTGTCGGCGTCCCTGG-3′; elastin reverse, 5′-AGCGGCTG-CAGCTGGAGGTA-3′ (354 bp); fibrillin 1 forward, 5′-CTTGAAGG-GAGAAGGCTGG-3′; fibrillin 1 reverse, 5′-AGGGACACTCGCAGCGATA-3′ (206 bp); β-actin forward, 5′-GCGA-GAAGATGACCCAGATC-3′; β-actin reverse, 5′-GGATAGCA-CAGCCTGGATAG-3′ (77 bp). Real-time polymerase chain reaction (PCR) was performed using the StepOnePlus real-time PCR system (Applied Biosystems, Foster City, CA, USA) with 1 μL of cDNA in a 20-μL reaction mixture containing 10 μL of the Power SYBR Green PCR Master Mix, 1 μL of each primer, and 7 μL of PCR-grade water (Thermo Fisher Scientific, Rockford, IL, USA). The reaction conditions were 95 °C for 10 min, followed by 40 cycles at 95 °C for 15 s and 60 °C for 1 min. The crossing points for the target genes were calculated, and the relative amounts were quantified.

### 2.7. Hematoxylin and eosin staining

The human skin equivalent treated with KRG was stained using hematoxylin and eosin (H&E) following standard procedures. The tissue was deparaffinized, rehydrated using ethanol, stained for 3 min using a hematoxylin solution (Sigma-Aldrich), and rinsed for 30 s using tap water. Next, the tissue was stained for 3 min using an eosin B solution (Sigma-Aldrich) and mounted by dehydration. The stained images were edited using an iScan HT digital pathology image scanner (Ventana Medical Systems, Tucson, AZ, USA).

### 2.8. Scanning electron microscopy

A paraffin block prepared for tissue staining was sliced into 5-μm thick sections and attached to a slide. Xylene and ethanol were each dripped onto the slide for 3 min to remove the paraffin. After removing all the paraffin, the slide was rinsed for 30 s using tap water. A platinum coating was applied around the tissue, according to the standard procedure for preparing biomaterial for electron microscopy. The nanostructure of the collagen fibers was visualized using scanning electron microscopy (SEM; Hitachi S-4700, Tokyo, Japan).

### 2.9. Atomic force microscopy

Nanoscale images of fibroblasts and collagen were obtained by AFM using a NANOStation II (Surface Imaging Systems, Herzogenrath, Germany). The force–distance (FD) curve was measured in contact mode. The contact probe consisted of a reflex-coated gold cantilever and tip (BudgetSensors, Sofia, Bulgaria). The specifications of the probe used in this study were as follows: cantilever dimensions, 450 × 50 × 2 $\mu m^3$ (length × width × thickness); force constant, 0.2 N/m; resonance frequency, 13 kHz; tip height, 17 μm; tip radius, <10 nm; and half cone angles at the tip, 20–25° along the cantilever axis, 25–30° from the side, and 10° at the apex. The probe loading rate and traveling distance were fixed at 1 μm/s and 2.3 μm, respectively.

### 2.10. Rheological measurements

Rheological properties of the human skin equivalent were measured using a discovery HR-2 rheometer (TA Instruments, Newcastle, PA, USA). Viscoelastic storage modulus ($G'$) and loss modulus ($G''$) were measured by strain sweeps. Samples were loaded onto the stage, and the spacing between the stage and the probe disk was constantly adjusted for all measurements. The strain swept from 0.01% to 1000.0% at an angular frequency of 10.0 rad/s. All experiments were carried out at a constant temperature of 23 °C.

### 2.11. Statistical analyses

All data were expressed as means ± standard deviations. Statistical analyses were performed using the two-tailed Student $t$ test (version 13; SPSS, Chicago, IL, USA). A $p$-value <0.05 was considered significant.

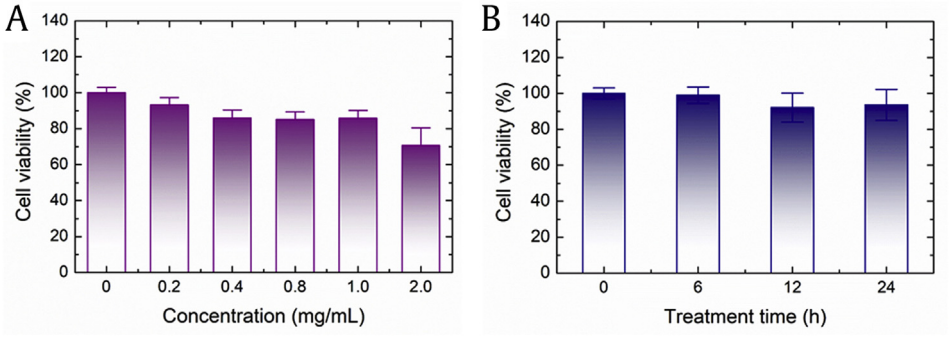


**Fig. 1.** A 3-(4,5-dimethylthiazol-2-yl)-2,5-diphenyl tetrazolium bromide (MTT) assay was used to evaluate the cytotoxicity of (A) various concentrations of red ginseng and (B) different treatment durations.

## 3. Results

### 3.1. Fibroblast viability as a function of KRG concentration and treatment time

Ginsenosides are the major pharmacological components of KRG. The KRG ginsenoside content was analyzed using UPLC and is summarized in Table 1. Changes in fibroblast viability induced by ginseng were evaluated using an 3-(4,5-dimethylthiazol-2-yl)-2,5-diphenyl tetrazolium bromide cell proliferation assay (Fig. 1A). Cell viability was assessed in triplicate for various ginseng concentrations and treatment durations, and the results were similar for each experiment. Compared with the controls, fibroblasts treated with ginseng had lower survival rates with all treatments. However, survival rates were not significantly different at concentrations up to 1.0 mg/mL, showing values $>$ 85% of those of controls. When the ginseng concentration was increased to 2.0 mg/mL, the fibroblast survival rate decreased to 70%, suggesting an increase in toxicity. Changes in cell viability induced by ginseng were also examined by varying treatment duration (0, 8, 16, and 24 h) with 0.8 mg/mL ginseng (Fig. 1B). Cell viability was slightly decreased with increasing treatment duration; however, this change was not significant.

### 3.2. Effect of KRG on cellular stiffness

Nanoscale fibroblast images were generated using AFM. A three-dimensional AFM image of a fibroblast is shown in Fig. 2A. The nucleus region is the thickest, and the cell becomes progressively thinner toward the outer edge. Elasticity was measured around the nucleus because this region contains most of the F-actin proteins, which is associated with cell stiffness. Because the stiffness of the basal surface (i.e., the culture dish) may be reflected in the FD curve if the cell membrane is too thin, the FD curve was measured in a peripheral region with a height of at least 1,000 nm, as indicated by the white arrows (Fig. 2A). Fig. 2B shows a typical FD curve, with the load force plotted as a function of the indentation depth. The curve with black rectangles corresponds to the approaching process, and the curve with red rectangles corresponds to the retracting process. Young's modulus for the fibroblasts was determined from the approaching curve based on the Sneddon model (Fig. 2C) [15]. A large Young's modulus corresponds to a stiff cell, whereas a small Young's modulus corresponds to a softer cell. Fig. 2D shows the distribution of Young's modulus as a function of ginseng concentration. There was a large variation in cellular stiffness, as indicated by the broad within-group distribution. At low ginseng concentrations ($\leq$0.4 mg/mL), there was no significant change in cellular stiffness (Fig. 2E). However, at high concentrations ($\geq$0.8 mg/mL), cellular stiffness decreased significantly. Cellular stiffness was reduced by 28% at 0.8 mg/mL and by 50% at 2.0 mg/mL KRG compared with the controls. This reduced stiffness indicates that the cells were more susceptible to deformation by external forces. Because the stiffness of the fibroblasts showed a significant change at 0.8 mg/mL, this concentration was used to investigate the effects of varying the duration of treatment. Fig. 2F shows cellular stiffness as a function of treatment duration at 0.8 mg/mL KRG. Cellular stiffness decreased only after 6 and 12 h of treatment and then recovered with further 18 and 24 h of treatments. However, the stiffness remained lower than in control cells.

### 3.3. KRG-induced changes in F-actin content

Actin is an abundant structural protein found in all eukaryotic cells and is associated with cellular stiffness. The monomeric form, known as G-actin, is the basic unit of actin filaments, known as F-actin, that are generated by the polymerization of G-actin monomers. We investigated the effects of KRG on the transition from G-actin to F-actin. Changes in the expression of G-actin and F-actin as a function of ginseng concentration are shown in Fig. 3A. The expression of both G-actin and F-actin decreased with increasing ginseng concentrations. The ratio of F-actin to G-actin in the control cells was 1.5 $\pm$ 0.5. This decreased to $<$ 1.0 at high ginseng concentrations (1.0 and 2.0 mg/mL) owing to a rapid reduction in F-actin content (Fig. 3B). The ratio of F-actin to G-actin also decreased with increasing treatment duration (Fig. 3C). When the cells were treated with 0.8 mg/mL KRG, the ratio of F-actin to G-actin

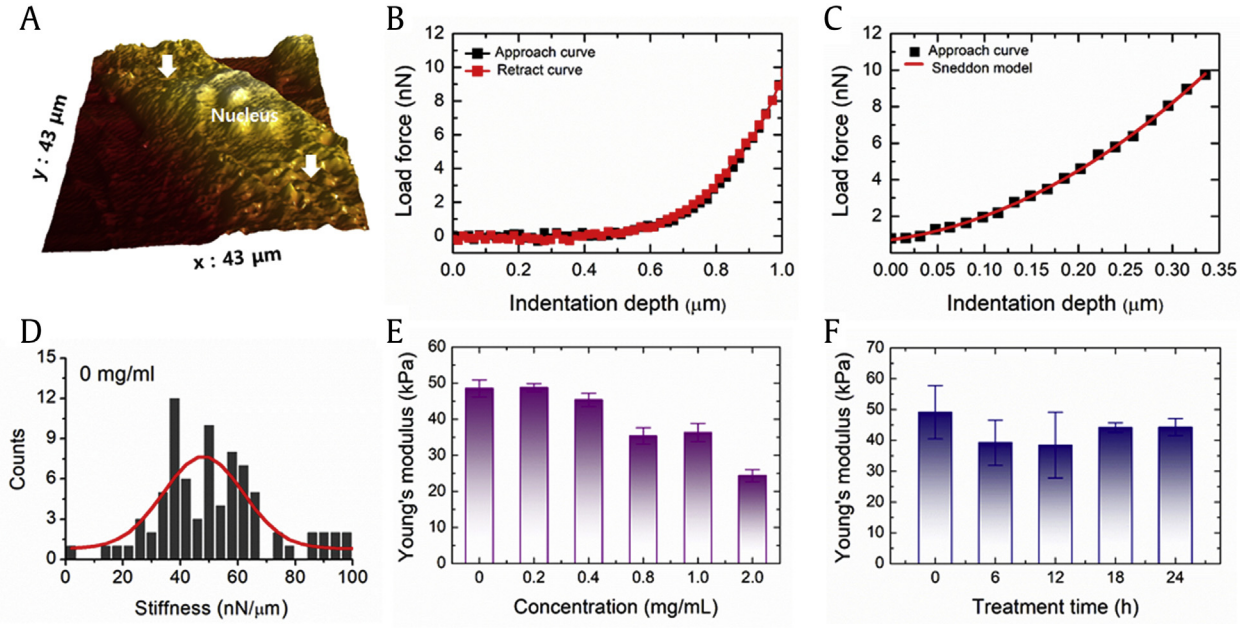


**Fig. 2.** (A) Representative topographical atomic force microscopy (AFM) image of a fibroblast. (B) The force–distance curve plotted as a function of load force and indentation depth and (C) the approach curve fitted to the Sneddon model. (D) Distribution of Young's modulus values for control fibroblasts. (E) Changes in Young's modulus for fibroblasts as a function of the red ginseng concentration and (F) treatment duration at 0.8 mg/mL.

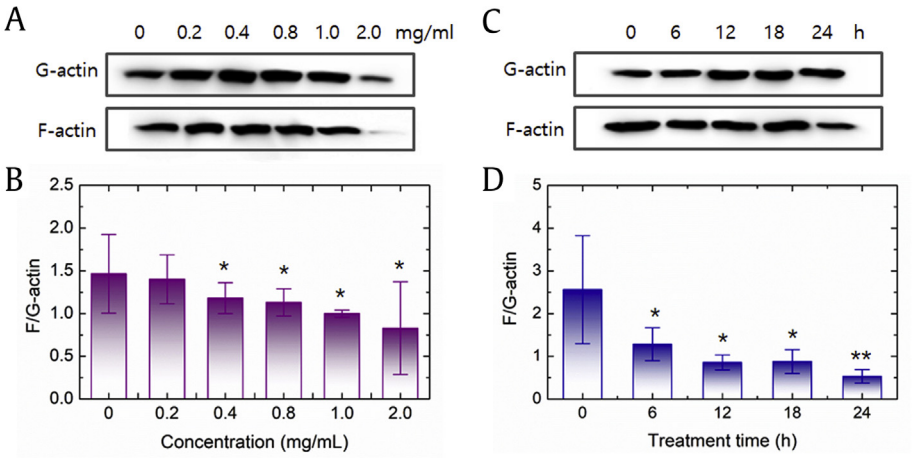


**Fig. 3.** (A) G-actin and F-actin protein expression according to red ginseng concentration. (B) Changes in the F-actin:G-actin ratio according to red ginseng concentration. (C) G-actin and F-actin protein expression according to treatment duration at 0.8 mg/mL red ginseng. (D) Changes in the F-actin:G-actin ratio according to treatment duration at 0.8 mg/mL red ginseng. $^{*}p < 0.05$ and $^{**}p < 0.01$ compared with the control.

decreased significantly after 6 h of treatment. This ratio had decreased to half the control value 6 h after the onset of treatment and continued decreasing thereafter (Fig. 3D). We measured the F-actin content twice at 0.8 mg/mL KRG and after 24 h of treatment. Compared with the control value, the F-actin content decreased 0.78-fold at the first measurement (Fig. 3A) and 0.2-fold at the second measurement (Fig. 3B). Each measurement was recorded three times, with similar results. The large difference between these two measurements may have been due to a lack of homogeneity among the cells or differences in the experimental conditions.

### 3.4. Effects of KRG on the expression of aging-related biomarker genes

The mRNA expression of aging-related biomarkers, including that of procollagen types I and VII, elastin, and fibrillin-1, was investigated at various ginseng concentrations. Compared with the controls, the expression of procollagen type I increased with 0.8 and 2.0 mg/mL KRG treatment; however, the mRNA expression level was unchanged with the other treatment concentrations (Fig. 4A). The expression of procollagen type VII was increased in response to KRG treatment, reaching significance at 2.0 mg/mL, where it was 8.8-fold higher than the control (Fig. 4B). The elastin expression level was decreased at 0.4 mg/mL KRG, and this decreased elastin level was maintained with 2.0 mg/mL KRG treatment (Fig. 4C). The mRNA expression of fibrillin-1 was increased by KRG concentrations higher than 0.8 mg/mL, reaching significance at 0.8 and 2.0 mg/mL (Fig. 4D). Overall, KRG treatment increased the procollagen type VII and fibrillin-1 expression level in fibroblasts, whereas that of elastin was decreased. In cells treated with 0.8 mg/mL KRG, mRNA expression levels of procollagen types I and VII were unchanged by short-term treatment ($\leq$12 h), but increased after 18 h of treatment (Fig. 4E and F). The mRNA expression levels of elastin and fibrillin-1 showed a similar pattern in response to treatment duration, gradually increasing to 18 h of treatment, but then stopped increasing or decreased slightly after 24 h (Fig. 4G and H).

### 3.5. Effects of KRG on collagen protein synthesis in fibroblasts and the skin equivalent

Living cells use mRNA to create their functioning protein molecules. During protein synthesis, mRNA transfers the information encoded in the DNA to the cytoplasm [16]. Therefore, we investigated whether changes in procollagen mRNA expression induced by KRG affect protein synthesis at the cell level and in the human skin equivalent by treating both fibroblasts and the human skin equivalent with varying KRG concentrations and treatment durations and then analyzing the expression levels of collagen proteins by Western blotting.

Overall, collagen type I protein synthesis was inhibited by KRG treatment. Although the expression of collagen type I protein increased at 0.2 mg/mL compared with the controls, the expression level decreased with increasing treatment concentrations (Fig. 5A, C). With a fixed KRG concentration of 0.8 mg/mL, the synthesis of collagen type I protein decreased in all the groups, regardless of treatment duration, and the decreasing rate showed no correlation with treatment duration (Fig. 5B and C). The expression of collagen type VII protein was increased with all KRG treatments, except at the 0.8 mg/mL concentration (Fig. 5D, F). This increase was significant at low concentrations (0.2 and 0.4 mg/mL). Compared with the control, collagen protein type VII synthesis was decreased after 6 h of treatment at 0.8 mg/mL; however, no additional significant changes were observed with increased treatment duration (Fig. 5E and F).

The tendency of collagen protein expression in the human skin equivalent was similar to that in fibroblasts. The expression of collagen type I protein was decreased at KRG treatment concentrations of up to 1.0 mg/mL (Fig. 5G, I), but increased slightly at 2.0 mg/mL. At 0.8 mg/mL KRG, collagen type I protein synthesis increased after 6 h of treatment, but decreased with longer treatment durations (Fig. 5H and I). Collagen type VII protein synthesis was increased by KRG treatment, and the increase was significant at concentrations of 0.2, 0.4, and 2.0 mg/mL (Fig. 5J, L). The effects of treatment duration were not significant for collagen type VII protein synthesis (Fig. 6K and L). This result indicates that the effect of KRG on collagen protein synthesis is transmitted to the skin equivalent.

### 3.6. Collagen fiber in the skin equivalent

To analyze changes in collagen fibers induced by KRG, the human skin equivalent was treated with varying KRG concentrations and treatment times and then analyzed by H&E staining. Increasing treatment duration resulted in a slight and insignificant change in collagen fiber staining (red staining), and we analyzed this change using ImageJ software (Fig. 6A). A darker red color indicates more

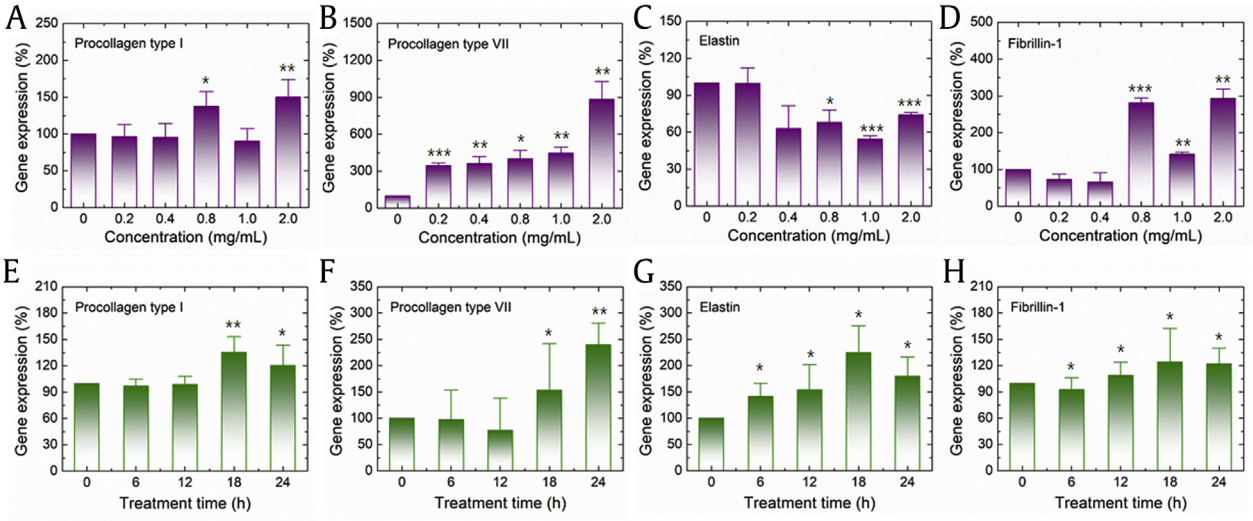


**Fig. 4.** Expression of (A) collagen type I, (B) collagen type VII, (C) elastin, and (D) fibrillin 1 mRNA according to red ginseng concentration. Expression of (E) collagen type I, (F) collagen type VII, (G) elastin, and (H) fibrillin 1 mRNA with different red ginseng treatment durations. $^{*}p < 0.05$, $^{**}p < 0.01$, and $^{***}p < 0.001$ compared with the control.

collagen or thicker collagen fibers. However, owing to the limited resolution, H&E staining did not show a change in collagen fiber thickness, suggesting that the color change may reflect a change in collagen density. The collagen density did not change with increasing KRG concentrations (Fig. 6B). Although the collagen density was decreased in the skin equivalent treated with 0.8 mg/mL KRG for 6 and 12 h (Fig. 6C), collagen density returned to the level observed in the control after 24 h of treatment.

To analyze changes in the structure, the collagen fibers were visualized using SEM and AFM (Fig. 6D and E). Collagen was visible as long fibers that formed partial bundles. The collagen fiber indicated by the arrow was selected, and its thickness was measured by SEM (Fig. 6D). No changes in thickness were recorded with KRG treatment concentration of up to 0.8 mg/mL, but marginal increases were observed at 1.0 and 2.0 mg/mL (Fig. 6F). When the skin equivalent was treated with 0.8 mg/mL KRG, the collagen fiber thickness increased with increasing treatment duration. At 0 h, the collagen fiber was 44.5-nm thick, which increased to 55, 59.5, and 60 nm at 6, 12, and 24 h, respectively. The three-dimensional collagen fiber structure was confirmed in the human skin equivalent image generated using AFM (Fig. 6E), where the nanostructure and organization of the collagen fiber are clearly visible. The collagen shows periodic banding at intervals of approximately 67 nm, known as D-banding. The changes in the thickness of the collagen fiber according to the duration of KRG treatment were also confirmed via the AFM images.

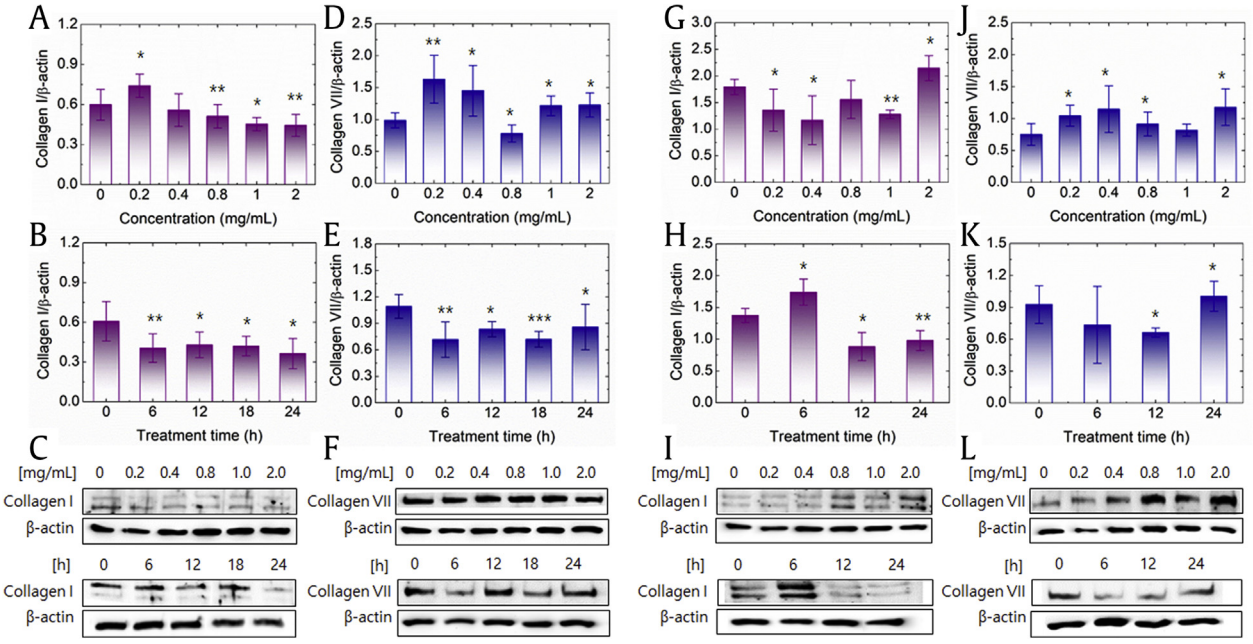


**Fig. 5.** (A) Collagen type I protein expression according to red ginseng concentration and (B) treatment duration. (C) Western blot of collagen type I protein in cells. (D) Collagen type VII protein expression according to red ginseng concentration and (E) treatment durations. (F) Western blot of collagen type VII protein in cells. (G–I) Collagen type I protein expression according to red ginseng concentration and treatment duration; (J–L) are the results for collagen type VII in the skin equivalent. $^{*}p < 0.05$, $^{**}p < 0.01$, and $^{***}p < 0.001$ compared with the control.

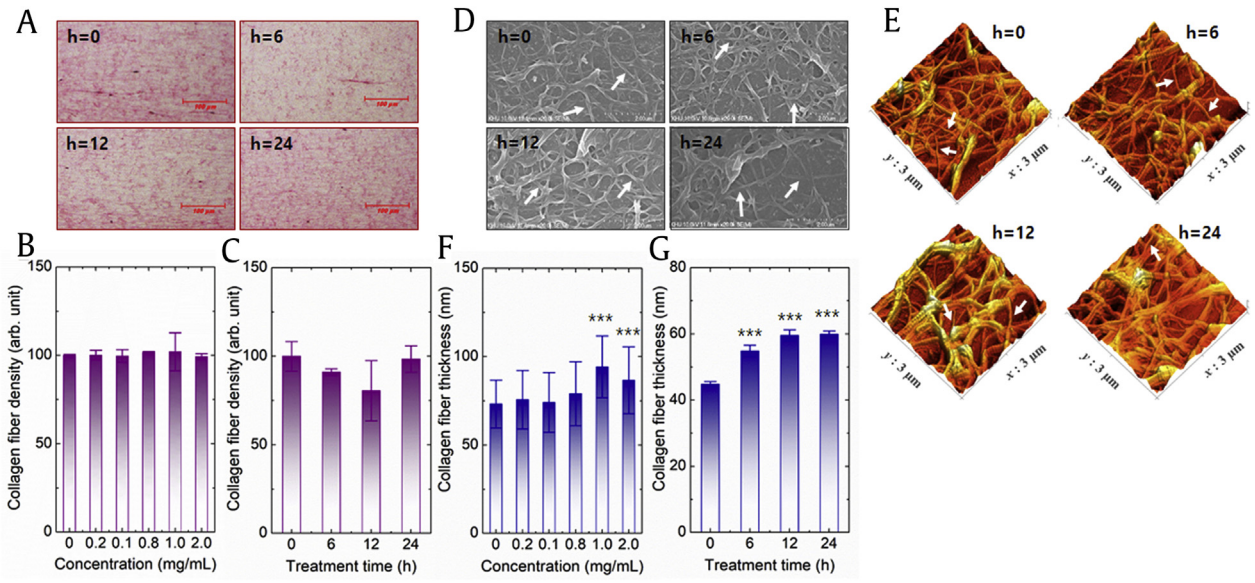


**Fig. 6.** (A) Human skin equivalent stained with hematoxylin and eosin. Collagen is stained red. (B) Collagen fiber density in the sample according to red ginseng concentration and (C) treatment duration. (D) Collagen was visualized using scanning electron microscopy (SEM). (E) Collagen fiber thickness measured in SEM images according to concentration and (F) treatment duration. (G) Collagen nanostructure in the sample treated with red ginseng (0.8 mg/mL) for 0, 6, 12, and 24 h visualized using atomic force microscopy.

### *3.7. Changes in viscoelasticity of the skin equivalent*

To investigate the effects of KRG on the viscoelastic properties of the skin equivalent, the strain modulus was determined by dynamic strain sweep. The skin equivalent was treated with varying KRG concentrations and treatment durations at 0.8 mg/mL KRG, and the effects of concentration and treatment duration on the viscoelastic properties were analyzed separately. When the strain amplitude value was less than 1%, the $G'$ and $G''$ curves of the KRG-treated skin equivalent were independent of strain and exhibited linear viscoelastic behavior (Fig. 7A and B). With an increase in strain amplitude, the $G'$ and $G''$ curves of all the skin equivalents decreased gradually, and the samples exhibited nonlinear behavior. In all samples, $G'$ was higher than $G''$ in the linear viscoelastic region, indicating a solid- or gel-like elastic behavior for all KRG-treated skin equivalents. Compared with the control, skin equivalents treated with 0.2–1.0 mg/mL KRG had lower $G'$ and $G''$ within the linear viscoelastic region. The skin equivalent treated with 2.0 mg/mL KRG had the highest $G'$ and $G''$ in the region, indicating that deformation resistance of the skin equivalent was reduced at KRG concentrations of up to 1.0 mg/mL. The enhanced deformation resistance with 2.0 mg/mL KRG treatment may be related to increased expression of collagen type I and VII proteins, although no clear changes in collagen fiber density were observed with microscopy analyses. The viscoelastic behavior of the skin equivalent did not change with treatment duration (Fig. 7C and D). The $G'$ and $G''$ curves were both lower with increasing treatment duration; however, the reduction was not significant.

## 4. Discussion

The structure, morphology, and mechanical properties of human skin change constantly with age. The outer epidermis becomes thinner, the number of wrinkles increases, and the skin loses its strength and elasticity owing to reduced production of collagen and elastin, as well as decreases in the density of the extracellular matrix [17,18]. Skin elasticity has been evaluated using several noninvasive methods based on different principles. Magnetic resonance and ultrasound elastography are used to measure elastic properties using shear wave dispersion inside the skin [19–21], while acoustic shockwave emission and suction applied to the skin are often used to evaluate skin elasticity [22,23]. However, these *in vivo* methods offer limited resolution for detecting small lesions and may be significantly affected by external factors, including the body mass index and degree of hydration [24]. Individual fibroblasts within the skin also exhibit significant changes in stiffness with age. Schulze et al. [25] examined the viscoelasticity of fibroblasts isolated from 14 human donors aged 27–80 years and reported that fibroblasts from older donors were more rigid than those from younger donors. In addition, Young's modulus for fibroblasts has been shown to increase with cell age [26]. Fibroblasts isolated from a 30-year-old donor exhibited the lowest Young's modulus value (12.68 kPa), whereas the largest Young's modulus value (16.59 kPa) was found in cells from a donor older than 60 years. The increased stiffness of older fibroblasts is associated with changes in actin polymerization. The elastic properties of fibroblasts are regulated by the cytoskeleton, which provides the cell with rigidity, shape, and integrity. The cytoskeleton consists of microtubules, actin filaments, and intermediate filaments, and these components have different functional and mechanical properties [27]. Enhanced actin polymerization can modulate the stiffness of cells, whereas dense, highly cross-linked F-actin networks increase cellular stiffness, resulting in cells that are less susceptible to deformation [28]. Actin polymerization is regulated by numerous actin-binding proteins and different signaling pathways [29], and G-actin concentration, ATP binding, and actin hydrolysis can all promote actin polymerization [30]. Aging results in changes to the cytoskeleton, leading to an increase in the polymerized F-actin:monomeric G-actin ratio. Compared with fibroblasts isolated from donors aged 20–27 years, the quantity of F-actin isolated from cells of donors aged 61–72 years increased by 31% [25]. To counteract aging, actin polymerization in cells can be inhibited by ginseng. The F-actin content of RAW 264.7 cells was decreased by treatment with the ginsenoside Rg3, a saponin extracted from ginseng [31]. Moreover, the F-actin:G-actin ratio was decreased in leptin-treated cardiomyocytes compared with the

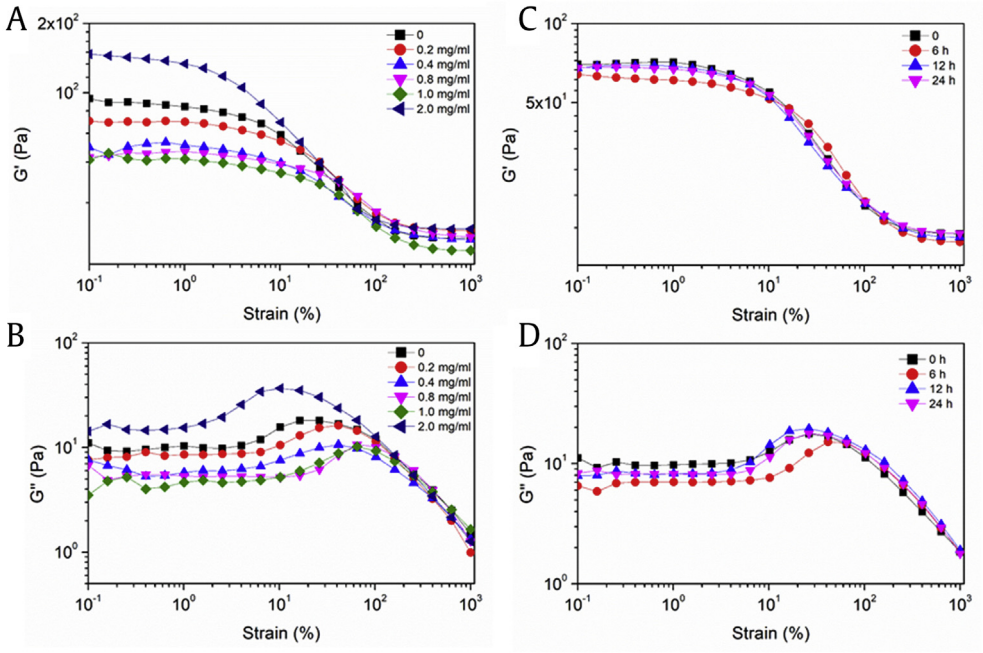


**Fig. 7.** Log profile of strain-dependent storage modulus ($G'$) and loss modulus ($G''$) for the skin equivalent. (A) $G'$ and (B) $G''$ curves according to red ginseng concentration. (C) $G'$ and (D) $G''$ curves according to treatment duration at 0.8 mg/mL red ginseng.

controls, indicating an increase in the quantity of F-actin [32]. In this study, we found that KRG induces changes in actin polymerization and cellular stiffness in fibroblasts. The F-actin level in fibroblasts decreased in response to KRG treatment, as shown in Fig. 3. Actin polymerization decreased significantly with increasing ginseng concentrations. This reduction in F-actin was reflected in the stiffness of the fibroblasts, as shown in Fig. 2E. As the quantity of F-actin decreased, the stiffness of the fibroblasts also decreased, resulting in cells that were more susceptible to deformation. These results suggest that cellular elasticity can be improved by KRG treatment and that this improvement can be quantitatively analyzed using AFM.

Collagen is the most abundant protein in human skin, maintaining its structure, smoothness, and elasticity [33]. The levels of collagen naturally decrease in aging skin [34]. There are 28 types of collagen, which can be subdivided into several groups based on the structure and supramolecular organization [34]. The collagen groups include fibril-forming, fibril-associated, network-forming, anchoring fibril, transmembrane, and basement membrane collagens. The fibril-forming collagen group is the most abundant, accounting for $>$ 90% of total collagen, and includes collagen types I, II, III, V, and XI. Collagen type VII belongs to the anchoring fibril group. The density, orientation, and thickness of collagen can all affect the elastic properties of skin. Procollagen is secreted by fibroblasts, and collagen is synthesized from procollagen by a complex sequence of intracellular and extracellular events. Many regulatory factors are involved in collagen synthesis, including ascorbic acid, glucocorticoids, amino-terminal propeptide, and membrane receptor systems [35]. We observed that the mRNA expression level of procollagen increased in response to KRG treatment, and the increase was significant for collagen type VII. Collagen synthesis showed a similar KRG dependency in both the cells and skin equivalent. Overall, the synthesis of collagen type I protein was inhibited by KRG treatment in both the cells and skin equivalent, except specifically for 0.2 mg/mL KRG in cells and 2.0 mg/mL in the skin equivalent. In contrast, the expression of collagen type VII increased with KRG treatment in both the cells and skin equivalent.

Changes in F-actin and collagen in the skin due to aging lead to changes in skin elasticity. According to Yoko et al. [36], skin deformation by suction using a Cutometer was less for elderly people than for young people, and the difference was more than two-fold. This result indicates that the elastic modulus of skin increases with aging. In this work, we demonstrated that the strain modulus of the skin equivalent decreased with KRG treatment, indicating that ginseng can restore skin elasticity. Although our results may not be quantitatively reproducible in human skin owing to the limitations of the skin equivalent model, the restoration of viscoelasticity by KRG treatment was clear. Therefore, we concluded that KRG can restore elasticity in human skin.

## 5. Conclusions

We investigated the effect of KRG on the elasticity of human skin. The stiffness of fibroblasts decreased in a concentration- and treatment duration–dependent manner in response to KRG treatment, and this decrease correlated with a decrease in F-actin content. Moreover, the viscoelasticity of the skin equivalent was rescued by KRG treatment, which was likely related to changes in both collagen protein synthesis and cellular stiffness.

## Conflicts of interest

The authors declare that they have no financial conflicts of interest.

## Acknowledgments

This work was supported by a 2017 grant from the Korean Society of Ginseng and funded by the Korea Ginseng Corporation and the National Research Foundation of Korea (NRF) grant funded by the Korea government (MSIT) (No. 2020R1F1A1057505). The authors thank the Korea Ginseng Corporation for providing ginseng powder and excellent assistance in the preparation of this study.

## References


[1] Ganceviciene R, Liakou AI, Theodoridis A, Makrantonaki E, Zouboulis CC. Skin anti-aging strategies. Dermatoendocrinol 2012;4:308–19.
[2] Kim J, Cho SY, Kim SH, Cho D, Kim S, Park CW, Shimizu T, Cho JY, Seo DB, Shin SS. Effects of Korean ginseng berry on skin antipigmentation and anti-aging via FoxO3a activation. J Ginseng Res 2017;41:277–83.
[3] Gunin AG, Petrov VV, Vasilieva OV, Golubtsova NN. Age-related changes of blood vessels in the human dermis. Adv Gerontol 2015;5:65–71.
[4] Sator PG. Skin treatments and dermatological procedures to promote youthful skin. Clin Interv Aging 2006;1:51–6.
[5] Diridollou S, Vabre V, Berson M, Vaillant L, Black D, Lagarde JM, Grégoire JM, Gall Y, Patat F. Skin ageing: changes of physical properties of human skin in vivo. Int J Cosmet Sci 2001;23:353–62.
[6] Cao J, Pham DK, Tonge L, Nicolau DV. Study of atomic force microscopy force–distance curves by simulation using the Connolly surface for proteins. Smart Mater Struct 2002;11:1–5.
[7] Cappella B, Dietler G. Force-distance curves by atomic force microscopy. Surface Science Reports 1999;34:1–104.
[8] Jerome G, Francis OS. The structure of human skin collagen as studied with the electron microscopy. J Exp Med 1948;88(5):555–68.
[9] Longo VD, Kennedy BK. Sirtuins in aging and age-related disease. Cell 2006;126:257–68.
[10] Watson RE, Griffiths CE, Craven NM, Shuttleworth CA, Kielty CM. Fibrillin-rich microfibrils are reduced in photoaged skin. Distribution at the dermal-epidermal junction. J Invest Dermatol 1999;112(5):782–7.
[11] Park SY, Shin YK, Kim HT, Kim YM, Lee DG, Hwang ES, Cho BG, Yin CS, Kim KY, Yi TH. A single-center, randomized, double-blind, placebo-controlled study on the efficacy and safety of "enzyme-treated red ginseng powder complex (BG11001)" for antiwrinkle and proelasticity in individuals with healthy skin. J Ginseng Res 2016;40:260–8.
[12] Jeong HC, Hong HD, Kim YC, Rhee YK, Choi SY, Kim KT, Kim SS, Lee YC, Cho CW. Quantification of maltol in Korean ginseng (Panax ginseng) products by high-performance liquid chromatography-diode array detector. Pharmacogn Mag 2015;11:657–64.
[13] Jeon JM, Choi SK, Kim YJ, Jang SJ, Cheon JW, Lee HS. Antioxidant and antiaging effect of ginseng berry extract fermented by lactic acid bacteria. J Soc Cosmet Sci Korea 2011;37:75–81.
[14] Lee CH, Kim HI, Kim JS, Oh MJ, Kim SW, Ma SY, Kim MS, Kwon J, Jeong HS, Oh CH. Morphological studies on the inhibitory effects of photoaging skin of fermented red ginseng in hairless mice. Korean J Orient Physiol Pathol 2014;28:206–16.
[15] Cappella B, Dietler G. Force-distance curves by atomic force microscopy. Surf Sci Rep 1999;34:1–104.
[16] Cole CN, Scarcelli JJ. Transport of messenger RNA from the nucleus to the cytoplasm. Curr Opin Cell Biol 2006;18(3):299–306.
[17] Yamauchi M, Woodley DT, Mechanic GL. Aging and cross-linking of skin collagen. Biochem Biophys Res Commun 1988;152:898–903.
[18] Quan T, Fisher GJ. Role of age-associated alterations of the dermal extracellular matrix microenvironment in human skin aging: a mini-review. Gerontology 2015;61:427–34.
[19] Zaleska-Dorobisz U, Kaczorowski K, Pawluś A, Puchalska A, Inglot M. Ultrasound elastography: review of techniques and its clinical applications. Adv Clin Exp Med 2014;23:645–55.
[20] Sarvazyan AP, Rudenko OV, Swanson SD, Fowlkes JB, Emelianov SY. Shear wave elasticity imaging: a new ultrasonic technology of medical diagnostics. Ultrasound Med Biol 1998;24:1419–35.
[21] Ophir J, Cespedes I, Ponnekanti H, Yazdi Y, Li X. Elastography: a quantitative method for imaging the elasticity of biological tissues. Ultrason Imag 1991;13:111–34.
[22] Woo MS, Moon KJ, Jung HY, Park SR, Moon TK, Kim NS, Lee BC. Comparison of skin elasticity test results from the ballistometer and cutometer. Skin Res Technol 2014;20:422–8.
[23] Bonaparte JP, Ellis D, Chung J. The effect of probe to skin contact force on cutometer MPA 580 measurements. J Med Eng Technol 2013;37:208–12.
[24] Li C, Guan G, Reif R, Huang Z, Wang RK. Determining elastic properties of skin by measuring surface waves from an impulse mechanical stimulus using phase-sensitive optical coherence tomography. J R Soc Interface 2012;9:831–41.
[25] Schulze C, Wetzel F, Kueper T, Malsen A, Muhr G, Jaspers S, Blatt T, Wittern KP, Wenck H, Käs JA. Stiffening of human skin fibroblasts with age. Biophys J 2010;99:2434–42.
[26] Ida DM, Monika P, Katarzyna P, Małgorzata L, Irena E, Małgorzata L. Age-related changes in the mechanical properties of human fibroblasts and its prospective reversal after anti-wrinkle tripeptide treatment. Int J Pept Res Ther 2014;20:77–85.
[27] Lomri A, Marie PJ, Escurat M, Portier MM. Cytoskeletal protein synthesis and organization in cultured mouse osteoblastic cells. Effects of cell density. FEBS Lett 1987;222:311–6.
[28] Fallqvist B, Fielden ML, Pettersson T, Nordgren N, Kroon M, Gad AKB. Experimental and computational assessment of F-actin influence in regulating cellular stiffness and relaxation behaviour of fibroblasts. J Mech Behav Biomed Mater 2016;59:168–84.
[29] Schaefer A, Te Riet J, Ritz K, Hoogenboezem M, Anthony EC, Mul FP, de Vries CJ, Daemen MJ, Figdor CG, van Buul JD, et al. Actin-binding proteins differentially regulate endothelial cell stiffness, ICAM-1 function and neutrophil transmigration. J Cell Sci 2014;127:4470–82.
[30] Dominguez R, Holmes KC. Actin structure and function. Annu Rev Biophys 2011;40:169–86.
[31] Huy TX, Reyes AW, Hop HT, Arayan LT, Min W, Lee HJ, Rhee MH, Chang HH, Kim S. Intracellular trafficking modulation by ginsenoside Rg3 inhibits Brucella abortus uptake and intracellular survival within RAW 264.7 cells. J Microbiol Biotechnol 2017 28;27:616–23.
[32] Moey M, Rajapurohitam V, Zeidan A, Karmazyn M. Ginseng (Panax quinquefolius) attenuates leptin-induced cardiac hypertrophy through inhibition of p115Rho guanine nucleotide exchange factor-RhoA/Rho-associated, coiled-coil containing protein kinase-dependent mitogen-activated protein kinase pathway activation. J Pharmacol Exp Ther 2011;339:746–56.
[33] Gelse K, Pöschl E, Aigner T. Collagens–structure, function, and biosynthesis. Adv Drug Deliv Rev 2003;55(12):1531–46.
[34] Angel P, Szabowski A, Schorpp-Kistner M. Function and regulation of AP-1 subunits in skin physiology and pathology. Oncogene 2001;20:2413–23.
[35] Pinnell SR. Regulation of collagen synthesis. J Invest Dermatol 1982;79(Suppl 1):73s–6s.
[36] Yoko A, Yoshiro Y, Yusuke D, Yoshinobu I, Shigehiro N. Analysis of viscoelasticity of human skin for prevention of pressure ulcers. J Mech Med Biol 2008;8:33–43.